

A Finite Element Analysis of Mid-Shaft Femoral Tolerance under Combined Axial-Bending Loading

Costin Untaroiu, Dan Genovese, Johan Ivarsson, Jeff Crandall
Center for Applied Biomechanics, University of Virginia

Abstract

Bone fractures occur frequently at mid-shaft femoral site during frontal and offset automotive crashes. Because these injuries are expensive, it is crucial to understand the injury mechanisms if this injury is to be prevented. The experimental investigation of femoral shaft tolerance under loading corresponding to real world accidents requires a challenging test setup that allows applying external loads in controlled conditions, mimics the boundary conditions of the femur, and measures the loads at the mid-shaft cross-section of the femur. In addition, the variability of mechanical and structural properties of the specimens complicates the determination of the injury tolerance of the femur under different loading conditions. A numerical alternative is presented in the current study. First, a subject specific finite element model of a femur is developed based on medical images. Then, the parameters of two material models frequently used to approximate the cortical bone properties are identified using the Successive Response Surface Methodology in the ranges reported in the literature. The objective function is defined based on the impact force data recorded during a three-point bending test and its corresponding numerical simulations. The polynomial meta-models implemented in LS-Opt converge at close values of the material parameters suggesting good performance of the heuristic design search in the current identification problem. The femoral tolerance at mid-shaft location is determined using a virtual test setup that applies combined axial –sagittal bending loading through an axial preload along the knee-hip line and a transversal impact load at the mid-shaft site along anterior-posterior or posterior-anterior directions. The femoral tolerance curves calculated based on external loads show sensitivity with respect to the impact direction of transversal load due to the initial curvature of the femur, but insignificant dependence on the material mode, or the failure criteria used for femoral cortical bone. In addition to suggesting a numerical approach that uses finite element simulations and optimization techniques to determine the injury tolerance of long bones, the results highlight the predominant role of the bending loading in a combined loading of the femur.

Introduction

Injuries to lower limb extremities are a common and expensive consequence of automotive frontal and offset crashes. Kuppa and Fessahaie (2003) examined the National Automotive Sampling System (NASS) database from 1993-2001 and found that the lower limb extremity was the most frequent injured body region, accounting for 36 % of all moderate-to-fatal injuries (AIS2+). A similar finding was also reported by Laituri et al (2006) who showed that the lower extremity is the most frequently injured body region for both belted and unbelted occupants involved in a frontal crash. Approximately half of the lower limb injuries are to the knee-thigh-hip (KTH) complex (Kuppa and Fessahaie, 2003) with a total estimated cost exceeding \$4.0 billion per year.

While the fracture of the femoral shaft is the most common KTH injury accounting for 31 % of all injuries (Rupp, 2006), the mechanism of this injury is not well understood. The likelihood of a front seat occupant sustaining a femoral shaft fracture in a frontal crash has traditionally been assessed by an injury criterion relying solely on the axial force in the femur (Viano 1977, Leung et al 1983, Mertz et al. 2003). However, recently published analyses of real world data (Laituri et al. 2006) indicate that femoral shaft fractures occur at axial loads levels below those found experimentally. These findings led Laituri et al. (2006) to hypothesize that these fractures may occur as a result of combined axial compression and externally applied

bending moment. An external moment in the femoral shaft of a driver could for example occur as a result of contact between the occupant's thigh and the lower rim of the steering wheel or due to orientation of the thigh/femur at the time of contact with the bolsters.

The current study uses finite element (FE) simulations to determine the tolerance of the human femoral shaft to the type of combined axial compression and bending loading of the front seat occupant's femur that may occur in a frontal crash. A subject-specific FE model of a human femur was developed from computer tomography (CT) scans of the femur. FE optimization techniques were used to identify the material parameters of the femoral cortical bone using test data recorded in a three-point bending impact test. Then, the tolerance of the human femoral shaft in combined axial compression and externally applied sagittal plane bending in the antero-posterior (AP) or postero-anterior (PA) direction were numerically investigated. The results show that the axial force applied along the knee-hip direction and its eccentricity relative to the centroid of mid-shaft femoral cross-section significantly contributes to the bending loading in the femoral shaft and consequently to the femoral shaft tolerance. It is believed that this study may help to better understand the loading in the femoral shaft under a combined loading and eventually, to assist in reconsidering the current injury criteria of femur used in impact tests.

Methods

Development of a Femur FE Model

The femur FE model used in this study was developed by Untaroiu et al. 2006 based on the CT (computer tomography) scans of a left femur specimen obtained from a 69-year-old male PMHS (163 cm height, 92 kg mass). Transverse contour lines for the exterior and interior surfaces of the femur were obtained using LabVIEW image analysis toolset (National Instruments, Austin, TX, ver. 7) and SurfDriver (Kailua, HI, ver. 3.5) based on the CT-Scan image files, with 1mm longitudinal resolution. In the epiphyseal regions of the femur, where the cortical bone layer is thin (1-2 mm), only the exterior contours were obtained and the interior region was considered as trabecular bone. The contour lines were then imported in Rhino-3D (Robert McNeel & Assoc., Seattle, WA, ver. 3.0), where NURBS (Non-Uniform Rational B-Spline) surfaces were reconstructed from the stack of planar contours (Figure 1.a).

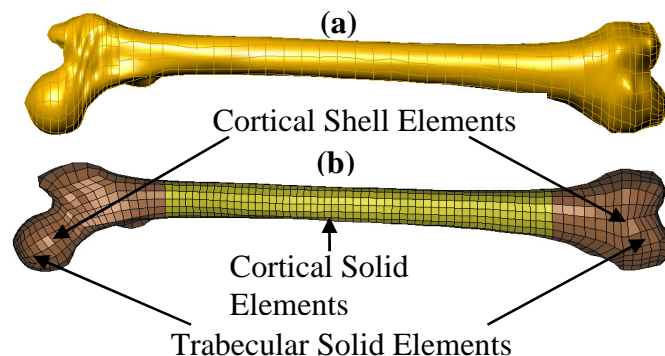


Figure 1. FE model of the dynamic three-point bend test of the femur (PA loading)

The FE mesh of femur (Figure 1 b) was generated using TrueGrid (XYZ Scientific Applications, Livermore, CA, ver. 2.2), which utilizes a “structural approach” to mesh complex three-dimensional objects using exclusively hexahedral solid elements. This process involved filling the solid objects, corresponding to various parts of the model, with cubic blocks (the mesh topology) and projecting the outer and inner boundaries to the exterior and interior surfaces of

the object. This approach provides advanced flexibility for increasing the mesh density during the verification of mesh convergence. Mesh convergence of an FE femur model in mid-shaft bending loading has previously been studied (Untaroiu et al. 2004) and it was found that femur FE models with two and four elements in the radial direction yielded almost identical results. The FE femur model in the current study was preliminarily simulated to verify the assumption that a two element cortical thickness was appropriate.

Material Identification of a Cortical Bone using FE Optimization Techniques

The parameters of cortical bone material models in the femur FE model were identified based on the test data of a dynamic three-point bending test performed on the femur specimen (Figure 2 a). In the testing the orientation of the bone was fixed by potting the bone in steel bone cups attached to rollers that acted as simple supports (Funk et al. 2004, Untaroiu et al. 2007). The posterior-anterior orientation of femur was defined by resting the bone on its most posterior protrusions (the medial/lateral condyles and the lesser trochanter) and aligning its most medial protrusions (the femoral head and the medial epicondyle). This provided contact between the femur and bone cups on the posterior, medial and inferior/superior surfaces. The same procedure was used for aligning the bone model within the modeled potting cups that were developed based on the geometry of the potting cups used in the experiments.

The steel potting cups and support plates were meshed with quadrilateral elements. The potting material was meshed with tetrahedral elements using Hypermesh (Altair, Troy, MI, ver.6.0) automatic mesh generator and its connections to bone ends and cups were created using shared-node interfaces. A 12-mm diameter cylindrical impactor, which in testing was attached to the crosshead of a universal test machine (model 8874, Instron, Canton, MA) and used to load the specimen in the mid-diaphysis, was modeled with solid elements. The FE femur model together with the FE models of test set-up components are illustrated in Figure 2 b.

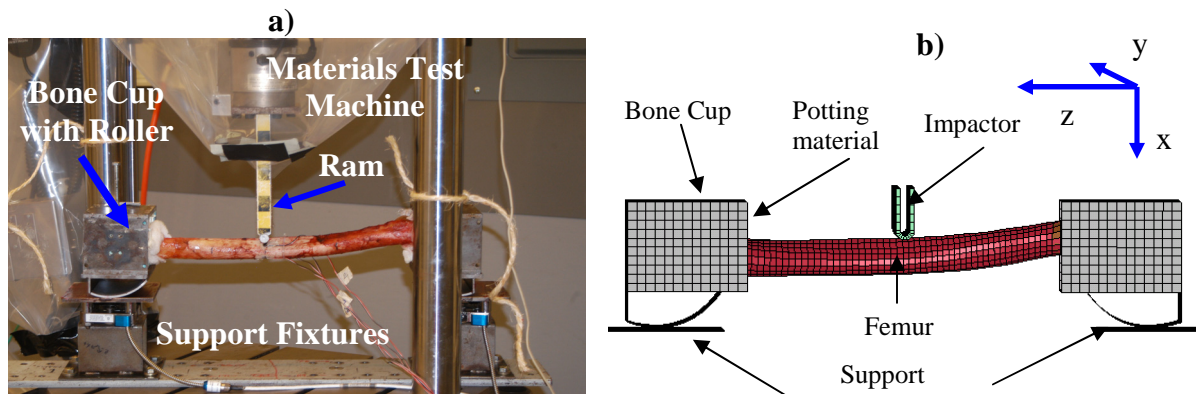


Figure 2. Three-point bend test of the femur (PA loading) a) physical test setup b) FE model of the test setup

Contact interfaces were defined between the rolling supports and bases. The rigid impactor was translated near the femur mid-shaft and a contact interface was created between them. The contact-impact algorithm of all contact definition used in the model was based on the penalty method (Hallquist 1998). The impactor was constrained to move only in the vertical direction and its displacement time-history was prescribed using the data measured with an accelerometer (which had been previously verified using a string potentiometer). The time-histories of contact forces were calculated at bone-impactor interface.

The material parameters of the cortical bone, for both material models, were obtained using the successive response-surface methodology (SRSM) implemented in LS-Opt (LSTC). Two constitutive models of cortical bone proposed in literature were considered for this study: isotropic elastic-plastic (EP-material #3 LS-DYNA), and elastic transversally isotropic (TI-material #2 LS-DYNA) and their parameter ranges were defined based on test data reported in the literature (Untaroiu et al. 2006). Cortical bone plasticity was assumed only for the EP model due to the lack of a transversally isotropic-plastic constitutive material model for solid elements in LS-DYNA. The objective function was chosen as root-mean-square (RMS) error between the impact force from the simulation and test data at equi-distant points of impactor displacement.

Injury Tolerance of Femoral Shaft under Combined Axial-Bending Loading using FE Analysis

The behavior and injury tolerance of the femur under combined axial-bending loading at the mid-shaft location was investigated using both FE femur models (EP and TI) validated in three-point bending test. A virtual test setup was defined in order to axially compress the femur and then to apply a bending moment in the sagittal plane (Figure 3). While it is well recognized that during a typical frontal crash the femoral axial loading is generated by the impact between the knee and the dashboard (States, 1986), the direction of impact force and the load transfer path are not well characterized. Therefore, the virtual test setup applied the axial load as a concentrated force through a node defined at the middle of femoral condyles (called the center of knee joint), and along a line which connects this point with the center of femoral head (the center of hip joint). As it can be observed (Figure 4), in unloaded configuration, the centroid of the femoral mid-shaft cross-section is eccentrically positioned with respect to the knee-hip axis, which implies that the axial load generates significant bending loading into the mid-shaft cross-section.

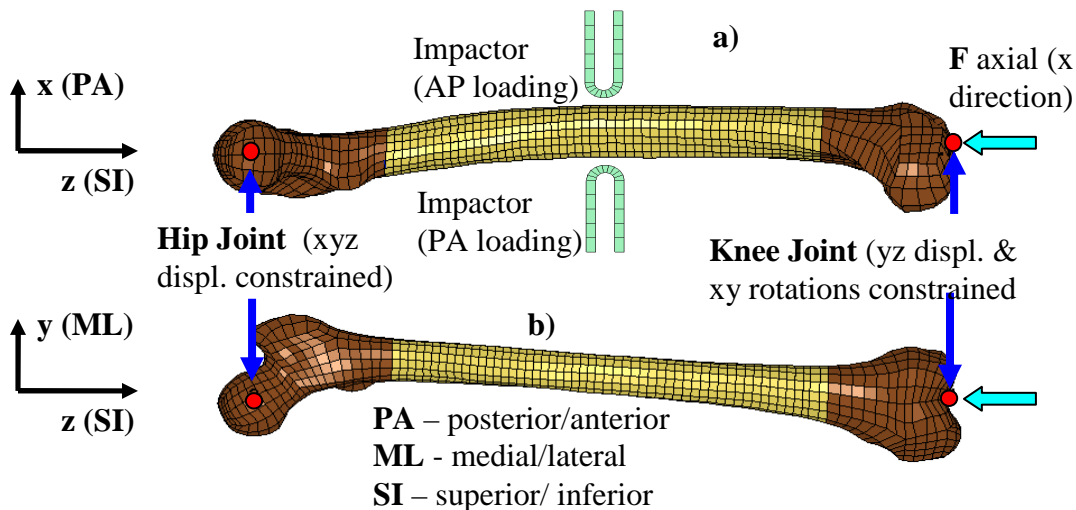


Figure 3. The femur FE model and the setup conditions used for combined loading tests. a) lateral view; b) anterior view

In order to avoid possible artifactual fractures caused by the axial loading approach (concentrated force) or by the simplifications used in the modeling of femoral end regions, the proximal and distal femoral ends were defined as rigid bodies. First, the distal and proximal regions were assumed as deformable parts, and their centers of mass and inertial properties (mass and mass moments of inertia) were calculated using preliminary FE simulations. Then, their mass moments of inertia were recalculated with respect to the centers of knee and hip joints

(centers of gravity of rigid parts) and were assigned to the femur model. While the proximal part of femur was allowed to rotate freely around the hip center that was considered fixed, the distal part of the femur was allowed to rotate only in the sagittal plane around the knee center and move along the direction of axial load.

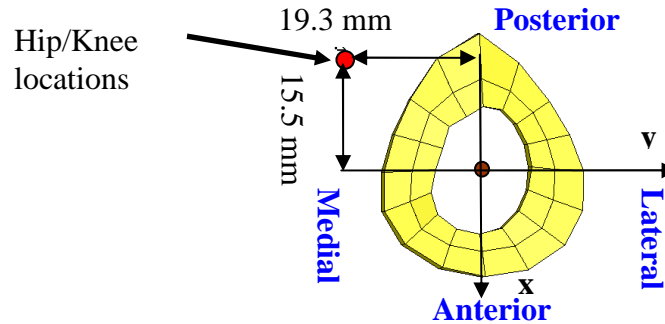


Figure 4. The cross-section of mid-shaft femur. The relative position of hip/knee joint to the area centroid

The femur models were subjected to a constant ramp of maximum compressive load and then hold until the failure. After the femur was loaded at maximum axial load (20 ms), the bending loading in sagittal plane was induced in the femoral shaft by loading the femur until failure with the same impactor used in three-point bending test at a constant velocity of 1.5 m/s at the mid-shaft in AP and PA direction. The bone failure was modeled in FE simulations using the element elimination technique that is based on the removal of elements whose stresses or strains reach pre-determined critical values. The most common failure criteria used in cortical bone FE models is based on the plastic strain (Takahashi et al. 2000, Untaroiu et al. 2005) and was used in the EP femur FE model. While the TI material model has no incorporated bone plasticity, a failure criterion based on a maximum value of von Mises stress was used. The pre-determined values of bone fracture were defined in the femur models based on the maximum plastic strain (0.57 %) or on the maximum von Mises stress (180 MPa) at the time of bone fracture in the three-point bending simulations of the EP model and, respectively the TI model. The axial load and bending moment in sagittal direction (M_z) were calculated in each simulation at the time of bone fracture in the mid-shaft cross-section. In addition, the bending moment were also calculated using the external forces (axial and impactor forces) as it is usually calculated in testing.

Results and Discussion

Material Identification of a Cortical Bone using FE Optimization Techniques

The optimized material parameters of the EP model were calculated using different polynomial meta-models (Table 3). It can be observed that the Young's modulus and yield stress converge to close values (less 1 % variation), but there are significant differences between the optimized tangent modulus and Poisson's ratio values (about 50 % variation in tangent modulus). The sensitivity of the identified material parameters to the type of surface approximation used in optimization can be explained by the general behavior of bone until failure and the objective function chosen in the optimization process. In the optimized models, it was observed that the bone behaves mostly elastically until failure (except only few regions close to the impactor which were in the plastic domain); therefore, the plasticity parameters (yield stress and tangent modulus) can influence only the final portion of the impactor force-deflection curve (Figure 4)

while the elastic modulus has the highest influence in three-point bending (Untaroiu et al. 2005). The optimized parameters of the TI material model using different starting points (the bone properties reported by Reilly and Burstein -1975 and Yoon and Katz -1976) are listed in the Table 4. The optimized elastic and shear moduli obtained by both methods have similar values (less 1 % variations). As in the EP model, larger variations of optimized Poisson's ratios may be caused by small contributions of these parameters to the system response (impactor force).

Table 3. Material Parameters of Elastic Plastic (EP) Model obtained by SRSM Approximations

Material Parameter (Units)	SRSM Approximations*			
	L	LI	E	Q
E (GPa)	14.635	14.644	14.624	14.628
σ_y (MPa)	133	132.6	133	132.9
E_t (MPa)	1024	1230	801	874
ν	0.3435	0.358	0.371	0.365
RMS Error	0.1386	0.1387	0.1387	0.1388

* - **L** – Linear; **LI** – Linear with interaction
E – Elliptic; **Q** - Quadratic

Table 4. Material Parameters of Elastic Transversely Isotropic (ETI) Model obtained by SRSM using different initial points

Material Parameter	SRSM (Reilly & Burstein - 1975)	SRSM (Yoon & Katz - 1976)
E_T (GPa)	11.477	11.447
E_L (GPa)	17.618	17.766
$G_{LT} = G_{TL}$ (GPa)	3.3	3.3
ν_{TL}	0.275	0.22
ν_{TT}	0.53	0.49
RMS Error	0.15518	0.15544

L – longitudinal axis of bone;
T – transversal/circumferential axis of bone

The final optimized parameters of EP and TI models were chosen as the set of parameters that gave the smallest RMS errors (Tables 3 and 4). The time histories of impact forces in the three-point bending test predicted by the optimized material models were compared to test data in Figure 8 a) and b), respectively. As can be observed, the responses of both models showed a good graphical and numerical ($R^2 > 0.985$) fit to the test data.

The main limitations of the FE identification approach used in this study may come from inherent modeling approximations of test setups or bone cortical models. While the surfaces of impactor-bone and cup-base contacts were lubricated with grease before testing and a constant friction coefficient of 0.05 (corresponding to the dynamic friction coefficient of steel-steel lubricated contact) was used in all contacts, the exact value of friction forces from testing were unknown. However, several simulations were run with values of friction coefficients between 0 and 0.1 and it was observed that the impactor forces have a very low sensitivity to the friction coefficient ($R^2 > 0.996$). In addition, an oscillation of about 330 Hz can be observed in the force response calculated from FE simulations (Figure 4). This inconsistency of model prediction with respect to experimental test data may be caused by the bone damping which was not defined in the models. It is also known that cortical bone has different properties in tension and compression. (Cowin 2001). Due to the lack of a material model in LS-DYNA which takes into account these differences, material models with similar tension/compression properties were used which influence the local properties of bone and consequently injury locations, but not the bone global behavior or injury tolerance.

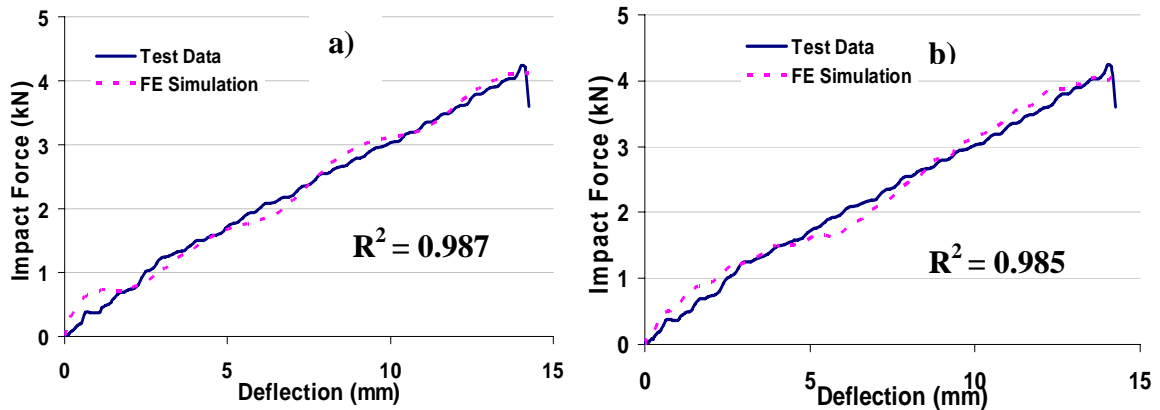


Figure 4. Force – deflection curves. Comparison between the test data and FE simulation results. a) Elastic-plastic (EP) model b) Elastic transversely isotropic (TI)

Injury Tolerance of Femoral Shaft under Combined Axial-Bending Loading using FE Analysis

The time histories of the sagittal bending moment in the mid-shaft femur (filtered using SAE 180 – SAE J21/1) depend on the direction of transversal loading (Figure 5a). While the initial bending moment generated by the compressive force during preloading is negative (Figure 5a) due to the initial eccentricity of the cross-sectional centroid (Figure 4), after applying the impactor load, the sagittal bending moment keeps or changes the moment sign depending on the direction of loading (PA or AP). The failure values of the sagittal bending moment in the mid-shaft cross-section shows close absolute values (Figure 5a), but the failure forces and impactor displacements are higher in AP loading that in PA loading (Figure 5b).

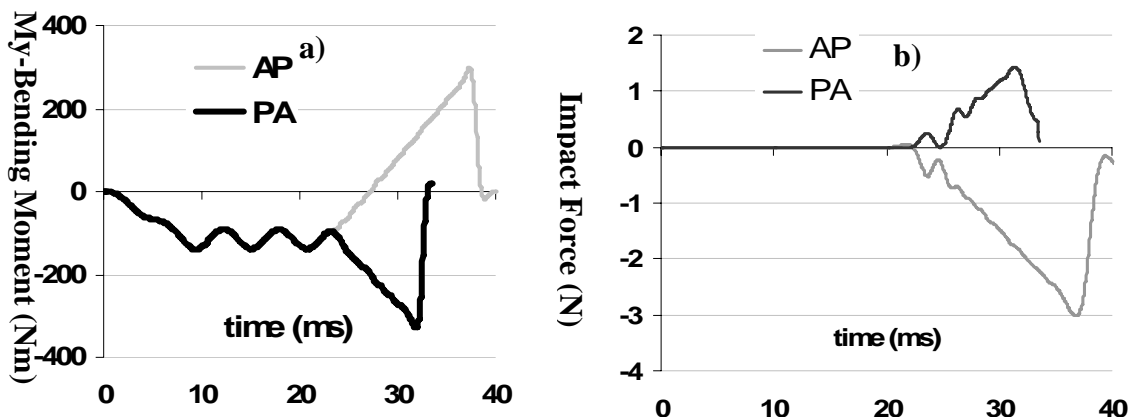


Figure 5. Comparison between the time histories of loading in PA and AP directions (6kN axial preload, EP model) a) bending moment in mid-shaft cross-section b) impact force

Initially, the compressive pre-load generates compression stresses on the anterior aspect of the femoral shaft and lower tensile stresses on the posterior aspect of the femoral shaft (Figure 5a). Then during applying the impactor load, the additional bending moment become predominant and generates compressive stress distribution on the impacted side of the femur (anterior side in AP loading – Figure 5a; posterior side in PA loading – Figure 5b), and tensile stress distribution on the opposite side.

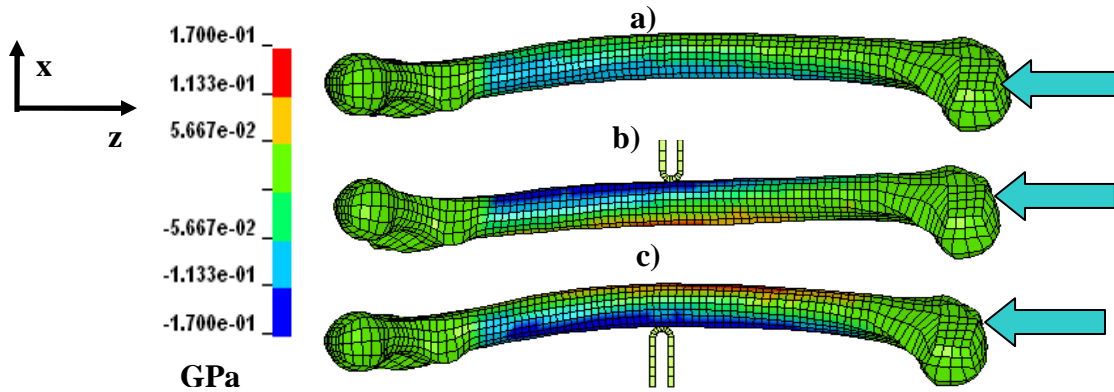


Figure 6. The longitudinal stress distribution in the FE femur (TI model) a) with axial preload (6kN) b) with axial preload and AP loading (before fracture) c) with axial preload and PA loading (before fracture)

The responses of femur models (EP and TI) under combined loading are similar in terms of the time histories of impactor force (Figure 6 a and b), but the TI model predicts the bone fracture at slightly higher loads than the EP model. While these differences can be caused by the unknown fracture mechanisms or the mesh sensitivity, the curves of femur tolerance show similar trends for different loading configurations (Figure 8 and 9).

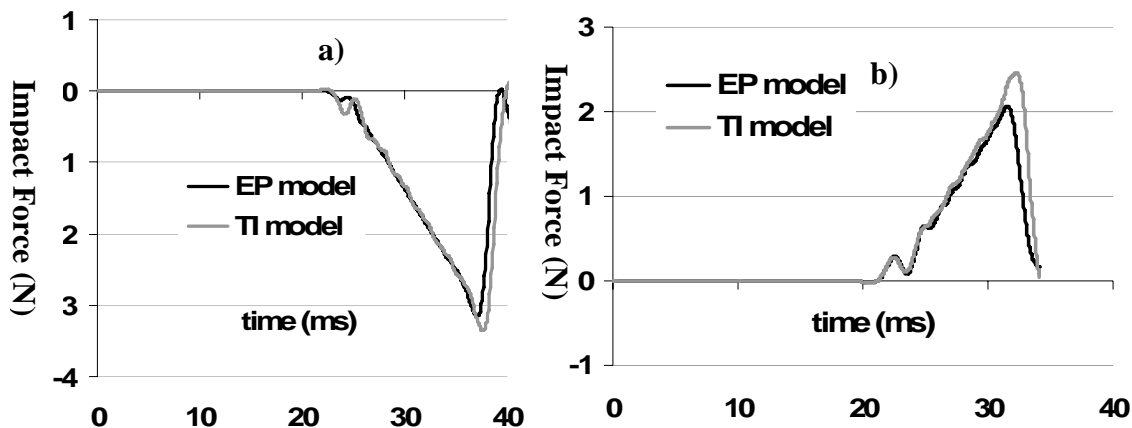
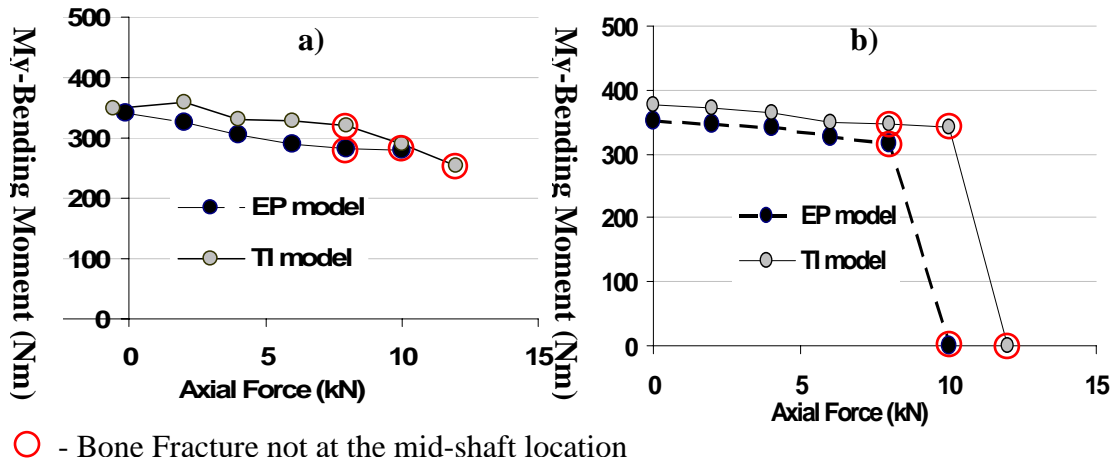


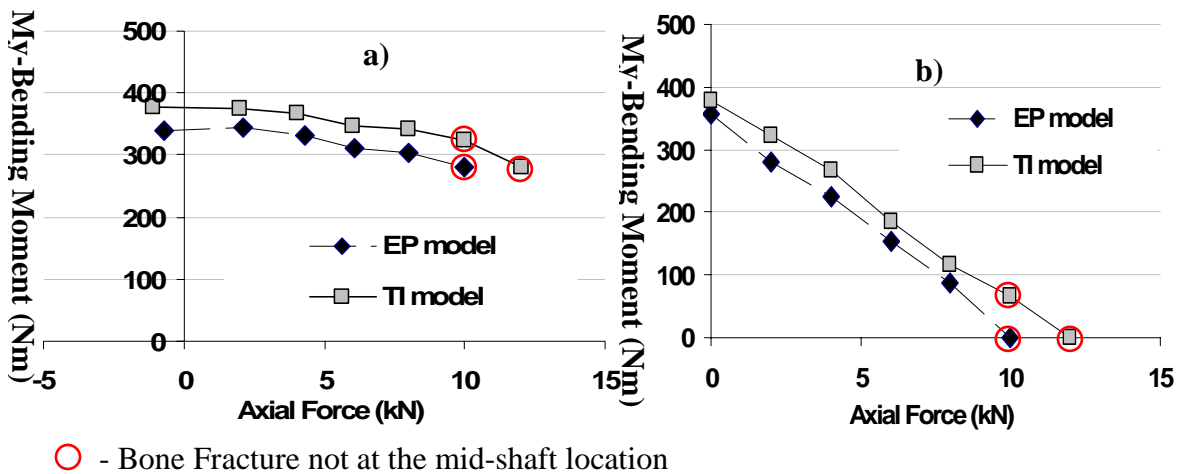
Figure 7. Comparison between the impact loadings obtained with EP and TI models (4 kN preload) a) PA impact direction; b) AP impact direction

The femur tolerance predicted by both cortical bone material models at various axial compressive preloads and AP loading are illustrated in Figure 8. The femur tolerance curves decrease slightly when the compressive load increases, suggesting that the stresses generated by the bending are much higher than the corresponding stresses of the axial load. In AP loading, the impactor load reduces the initial curvature of the femur relative to the axis of compressive load, and the failure usually appears at femur configuration close to a straight beam (Figure 5b). As a consequence, only a slightly difference in the femur tolerance curves calculated at the mid-shaft cross-section (Figure 8a) and the corresponding curves calculated based on external loads (Figure 8b) are observed. While at compressive preloads under 8 kN the first sites of bone fracture were close to mid-shaft (under the impactor), at higher loads the initial fracture appeared close to the connections between femoral shaft and bone ends (rigid parts). Therefore, the mid-shaft tolerances at these loadings are slightly underestimated. When high compressive preloads were applied (10 kN – EP model and 12 kN – TI model), the bending moments generated by axial force were sufficient to generate bone fractures without being loaded by the impactor.



○ - Bone Fracture not at the mid-shaft location
Figure 8. The femur tolerance (anterior/posterior-AP loading direction) a) calculated in mid-shaft cross section; b) calculated from exterior loading (straight beam theory)

The femur tolerance predicted by both cortical bone material models at various axial compressive preloads and PA loading are illustrated in Figure 9. While the tolerance curves based on the load distribution in mid-shaft cross-section at fracture are slightly similar in both cases (AP and PA) (Figure 9a), the tolerance curves based on the bending moment calculated using the external loads have accentuate descendent trend in PA loading (Figure 9b). Due to the initial curvature of the femur, toward the anterior direction (Figure 5c), the initial bending moment generated by the compressive axial load has the same sign as the bending moment developed by the impactor which imply a decreased tolerance of the femur in AP loading than in PA loading at a certain compressive preload. As in AP loading, high compressive preloads (10 kN –EP model, and 12 kN AP model) generate the bone fractures before applying the impactor force. In addition, the fracture sites at these high preload appear at the connections of bone with the shaft suggesting that the mid-shaft tolerance is underestimated at these axial loads.



○ - Bone Fracture not at the mid-shaft location
Figure 9. The femur tolerance (posterior/anterior-PA loading direction) a) calculated in mid-shaft cross section; b) calculated from exterior loading (straight beam theory)

Conclusions

Bone fracture in the femoral shaft is a lower limb injury that occurs frequently during frontal automotive crashes. While the mechanism of this injury is poorly understood, the current study

proposed a numerical investigation of femoral shaft tolerance using a subject specific finite element model of the femur to support the idea that combined loading is responsible for injuries. An inverse finite element approach was successfully used to identify the best parameter set of two bone material models from the test data of a three-point bending test performed on the femur modeled in this study. The Successive Response Methodology implemented in LS-Opt together with the defined objective function converged at similar values of material parameters showing insensitivity relative to the chosen polynomial meta-model or the starting point. The femoral tolerance at the mid-shaft location was determined using a virtual test setup which applies a combined axial–sagittal bending loading through an axial preload along the knee-hip line and a transversal impact load at the mid-shaft site along anterior-posterior(AP) or posterior-anterior(PA) directions. The femoral tolerance curves calculated based on external loads show sensitivity with respect to the impact direction of transversal load due to the initial curvature of the femur, but insignificant dependence on the material model, or the failure criteria used for femoral cortical bone. In addition to suggesting a numerical approach which uses finite element simulations and optimization techniques to determine the injury tolerance of long bones, the results highlight the role of bending in generating the mid-shaft stress and strain distribution during combined loading of the femur. This finding together with the test data of additional tests may be used in redefining the current injury criteria of femur used in anthropometric test devices, to index both force and moment terms.

References

1. Kuppa, S., Fessahaie, O. (2003) “An Overview of Knee-Thigh-Hip Injuries in Frontal Crashes in the United States,” Proceedings of the 18th International Technical Conference on the Enhanced Safety of Vehicles (ESV), Paper No. 416. National Highway Traffic Safety Association, Washington, DC.
2. Laituri, T., Henry, S., Sullivan, K., Prasad, P. (2006) “Derivation and Theoretical Assessment of a Set of Biomechanics-based, AIS2+ Risk Equations for the Knee-Thigh-Hip Complex,” Stapp Car Crash Journal, Vol. 50, pp. 97-130.
3. Rupp, J., Reed, M., Van Ee, C. (2002) “The Tolerance of the Human Hip to Dynamic Knee Loading,” Stapp Car Crash Journal, Vol. 46, pp. 211-228.
4. Viano, D. (1977) Considerations for a femur injury criterion. Proceedings 21st Stapp Car Crash Conference, pp. 443-473, SAE Paper No. 770925.
5. Leung, Y., Hue, B., Fayon, A., Tarrierre, C., Hamon, H., Got, C. (1983) Study of KTH protection criterion. Proceedings 27th Stapp Car Crash conference. Paper No. 831629.
6. Mertz, H., Irwin, A., Prasad, P. (2003) Biomechanical and scaling bases for frontal and side impact injury assessment reference values. Stapp Car Crash Journal, Vol. 47, pp. 155-188.
7. Untaroiu, C., Darvish, K., Crandall, J., Deng, B. and J.T. Wang, 2004. “Development and Validation of a Finite Element Model of the Lower Limb”, IMECE 2004-61583, 2004 ASME International Congress, Anaheim, CA, US.
8. Funk J.R., Kerrigan J.R, and Crandall J.R. (2004). “Dynamic Bending Tolerance and Elastic-Plastic Material Properties of the Human Femur”. 48th Proceeding of AAAM.
9. Hallquist, J. O., May (1998). LS-DYNA Theoretical Manual
10. States, J. (1986) “Adult Occupant Injuries of the Lower Limb,” SAE Paper No. 861927
11. Untaroiu, C., J. Kerrigan, and J. Crandall. (2006). “Finite Element Analysis of the Human Femur during Three-Point Bending Loading: Material Identification using Response Surface Methodology”. Paper 2006-01-0063 SAE Congress 2006.
12. Takahashi, Y.; Y. Kikuchi; A. Konosu and H. Ishikawa, (2000). “Development and Validation of the Finite Element Model for the Human Lower Limb of Pedestrians.” Stapp Car Crash Journal, 44, 2000-01-SC22.
13. Untaroiu C., Darvish K., Crandall J., Deng B., and J.T. Wang, (2005). “A Finite Element Model of the Lower Limb for Simulating Pedestrian Impacts”, Stapp Car Crash Journal, 49
14. Yoon, H.S. and Katz J.L. (1976), “Ultrasonic wave propagation in human cortical bone: II. Measurements of elastic properties and micro-hardness. J. of Biomechanics, 9, 459-464
15. Reilly, D.T. and Burstein A.H. (1975). “The elastic and ultimate properties of compact bone tissue”, J. of Biomechanics, 8, 393-405
16. Cowin S.C. (2001) Bone mechanics handbook, CRC Press.